The Absorber Layer Variation Effect on the Performance of FASnX₃-Based Perovskite Solar Cell

Setianto Ramaputra^{1,2}, Rossyaila Matsna Muslimawati³, Mohammad Kemal Augusta⁴, Muhammad Haris Mahyudin^{4,*}

¹Master Program of Engineering Physics, Faculty of Industrial Technology, Institut Teknologi Bandung, Jl. Ganesha No. 10 Bandung 40132, Indonesia.

²PT PLN Nusantara Power Unit Pembangkitan Muara Karang, Jl. Pluit Karang Ayu Barat No.1, Jakarta Utara 14450, Indonesia

³Doctoral Program of Engineering Physics, Faculty of Industrial Technology, Institut Teknologi Bandung, Jl. Ganesha No. 10 Bandung 40132, Indonesia

⁴Quantum and Nano Technology Research Group, Faculty of Industrial Technology, Institut Teknologi Bandung, Jl. Ganesha No. 10 Bandung 40132, Indonesia *Email: mahyuddin133@itb.ac.id

Abstract. The crucial need to eliminate harmful lead from extensively utilized metal halide perovskite solar cells (PSCs) necessitates the creation of practical and dependable lead-free perovskite alternatives. This research examines the performance of lead-free, hybrid organic-inorganic FASnX₃-based PSCs utilizing SCAPS-1D and VASP. The solar cell architecture used in this study is FTO/TiO₂/FASnX₃/PTAA/Au (X = Br, Cl). The results show that absorber layer FASnBr₃ has the highest power conversion efficiency of 19.67%, making it a good contender for improving perovskite solar cell performance. This work advances current experimental initiatives by suggesting an innovative device architecture and certain parameters, thereby offering an original strategy for optimizing the design of lead-free perovskite solar cells and facilitating future research in this field.

Keywords: Absorber layer, lead-free, $FASnX_3$ -based perovskite solar cell, $SCAPS\ 1$ -D, solar cell performance.

1 Introduction

Solar cells comprised of organic and inorganic components have lately emerged as a potential photovoltaic technology due to their low production costs, advantageous light absorption, adjustable absorption coefficient, longer diffusion length, and significant improvement in efficiency [1-4]. Perovskites are composed of the chemical formula ABX₃, where A is organic, inorganic, or mixed monovalent cations (e.g., CH₃NH₃⁺ (MA⁺), CH(NH₂)₂⁺ (FA⁺), and Cs⁺), B is metal divalent cations (e.g., Pb²⁺, Sn²⁺, Yb²⁺), and X (e.g., Br⁻, Cl⁻, and I⁻) are halogen anions. These materials have advantageous optical-electrical properties that make them suitable for use in photovoltaic (PV) systems, such as a sufficient and tuneable energy band gap, significant optical absorption, low electron and

Received ______, Revised _____, Accepted for publication _____ Copyright © xxxx Published by ITB Journal Publisher, ISSN: xxxx-xxxx, DOI: 10.5614/xxxx hole effective masses, high charge carrier mobilities, and long charge diffusion lengths [5]. Perovskite solar cells have garnered significant attention because their power conversion efficiency (PCE) has dramatically improved, increasing from 3.8% [6] to 25.7% [7].

Lead halide perovskite solar cells are becoming increasingly popular due to their inexpensive cost, excellent band gap, high absorption coefficient, and long carrier diffusion length [2]. Lead-based metal halide perovskites are recommended for this application due to their high efficiency. Lead-based PSCs are exciting research that has achieved the highest photovoltaic performance of 25.2% over the previous fifteen years [8]. However, lead toxicity causes significant environmental damage, and recycling such a heavy metal is complex and expensive. As a result, it is paramount to discover appropriate low-toxic or nontoxic metal ions to substitute lead in Pb-based perovskite materials [9].

Lead-free perovskite materials such as Ag, Bi, Cu, Ge, Sb, and Sn show promise as replacements for Pb, but their performance remains inferior to that of Pb [10]. Many studies have concentrated on MASnI₃ perovskite as the absorber layer for PSC [15-18]. Although previous studies have demonstrated that MASnI₃ has high mobility and a low effective mass [18], its efficiencies and stabilities are lower than those of MAPbI₃ perovskite solar cells due to the high sensitivity of Sn-based perovskites to oxygen and atmospheric moisture, which allows for easy oxidation of Sn²⁺ to Sn⁴⁺. This instability of Sn²⁺ in Sn-based perovskite may result in a structural alteration, lowering MASnI₃'s photovoltaic performance [19]. Koh et al. recently observed that replacing the MA cation with an FA cation increased the band gap to 1.41 eV [20], and FASnI₃ had greater mobility and thermal stability than MASnI₃.

The highest recorded enhanced electric field eco-friendly inorganic perovskite experiment, FASnI₃, stands at 13,82% [22] with an inverted planar solar cell structure of ITO/PEDOT:PSS/FASnI₃ gradient absorber/C₆₀/BCP/Ag. The FASnI₃ gradient devices had PCEs of 13.61% and 13.82%, with J_{SC} of 22.87 and 22.74 mA cm⁻², V_{OC} of 0.84 and 0.85 V, and FF of 70.9% and 71.5% under the forward and reverse scans, respectively. As a result, various interface layer adjustments are required to generate stable and efficient PSCs.

Studies that simulate and fabricate $FASnI_3$ with a 1.3-1.4 eV band gap have been carried out by many researchers [22-26]. Only a handful of researchers have conducted experiments with $FASnBr_3$ and $FASnCl_3$ absorber layers since their band gap falls into the wide band gap perovskites. These perovskite materials have a bandgap energy (E_g) > 1.7 eV, enabling them to absorb higher-energy (shorter wavelength) photons. This characteristic allows for efficient conversion of high-energy photons into electricity in photovoltaic devices. However, low-

energy photons do not absorb and pass through the wide bandgap perovskite layer, limiting the efficiency of wide bandgap perovskite solar cells. Despite the efficiency limitations imposed by their high band gaps, wide band gap perovskite solar cells may achieve respectable efficiencies, often in the 20% to 25% range [11]. This is especially notable as the theoretical efficiency ceiling for any solar cell is 33.7%. (attained with an ideal bandgap value of 1.34 eV).

In this study, we simulate a PSC structure of FTO/TiO₂/FASnX₃/PTAA/Au (X = Br, Cl) using the one-dimensional solar cell capacitance program (SCAPS-1D) and density functional theory (DFT) to better understand the distinct performance of certain materials and how they affect performance criteria. In addition, we investigate various approaches to obtain high efficiency in Pb-free perovskites. We discover that FASnBr₃ outperforms FASnCl₃.

2 Methodology

2.1 Computational Models

The basic physical parameters used for each layer variation were derived from various experimental and theoretical research [23–26]. As shown in Figure 1a, this study uses PTAA as the Hole Transport Layer (HTL) material, FASnI₃ as the absorber layer material, TiO₂ as the Electron Transport Layer (ETL) material, FTO as the front contact, and Au as the rear metal contact. PSC performances were explored using Prof. Mark Burgelman's SCAPS-1D version 3.3.10 [28-32].

The basic structure of FASnI₃ from previous work by Kahmann et al. [27] was utilized to calculate DFT on FASnBr₃ and FASnCl₃ structures by altering the halogen anion to Br and Cl. The optimized band structures of FASnBr₃ and FASnCl₃ (Figures 1b and 1c) were then used as input parameters in the SCAPS simulation to determine which structure generated the highest performance in production-ready PSC.

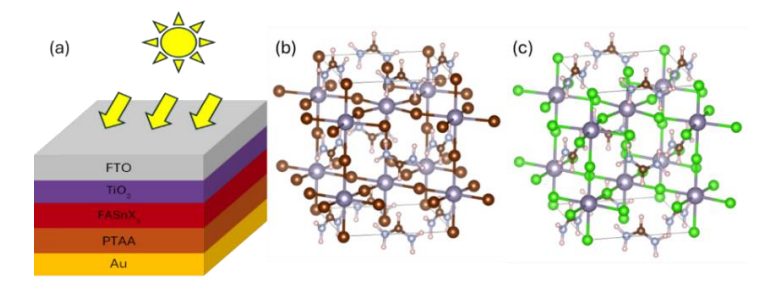


Figure 1 (a). Device simulation architecture. (b) FASnBr₃ and (c) FASnCl₃ optimized geometries using DFT+U.

2.2 Simulation Setup

The device simulations were performed by altering the thickness of FASnX₃ (X = Br, Cl) between 100 and 600 nm, as well as the absorber layer's defect density and the defect interface between HTL and ETL absorber layers. During simulations, charge carriers maintained a steady thermal velocity of 10^7 cm s⁻¹. The perovskite layer maintains its characteristics with a radiative recombination coefficient of 3×10^{-11} cm³ s⁻¹, an Auger electron capture coefficient of 1×10^{-29} cm⁶ s⁻¹, and an Auger hole capture coefficient of 1×10^{-29} cm⁶ s⁻¹ [33].

Table 1, obtained from diverse sources [23-26], outlines the physical characteristics applied for each layer's variations. Table 2 shows the interface defect parameters of Sn-based PSCs.

Material Properties	PTAA	FASnI ₃	TiO ₂	FTO
	(Ravishankar	(Almufarij et	(Hosen et al,	(Kumar et
	et al, 2022)	al, 2023)	2023)	al, 2020)
Thickness (nm)	10	500	50	500
Energy Bandgap (eV)	3.2	1.41	3.2	3.6
Electron affinity (eV)	2.13	4.47	4.1	4.1
Dielectric Permittivity	3	8.2	55	10
CB effective DOS (cm ⁻³)	2 x 10 ¹⁸	2.2 x 10 ¹⁸	1 x 10 ²¹	2.2 x 10 ¹⁸
VB effective DOS (cm ⁻³)	2 x 10 ¹⁸	1.8 x 10 ¹⁹	2 x 10 ²⁰	1.8 x 10 ¹⁹
Electron mobility (cm ² /Vs)	10-5	1.6	0.006	100
Hole mobility (cm ² /Vs)	10-5	1.6	0.006	25
Donor density (cm ⁻³)	0	1.0 x 10 ¹³	1.0×10^{19}	1.0 x 10 ¹⁹
Acceptor density (cm ⁻³)	1.0×10^{17}	1.0 x 10 ¹⁴	0	0
Defect type	Single Donor	Neutral	Single Acceptor	Neutral
Nt (cm ⁻³)	1.0 x 10 ¹³	1.0 x 10 ¹⁵	1.0 x 10 ¹⁵	1.0 x 10 ¹⁵

Tabel 1 The basic parameters utilized in the simulation

Tabel 2 Interface defect parameters used for the simulation

Parameters	Absorber/HTL	ETL/Absorber Neutral	
Defect type	Neutral		
Capture cross section electron (cm ⁻²)	1 x 10 ⁻¹⁵	1 x 10 ⁻¹⁵	
Capture cross section holes (cm ⁻²)	1 x 10 ⁻¹⁵	1 x 10 ⁻¹⁵	
Reference of defect energy level	Above the highest Ev	Above the highest Ev	
Energy distribution	Single	Single	
Energy with respect to reference (Ev)	0.60	0.60	
Total density (cm ⁻³)	1 x 10 ¹⁴	1 x 10 ¹⁴	

The absorber layer's band gap was computed using VASP (Vienna Ab initio Simulation Package). Spin-polarized DFT calculations were carried out with relaxed spin-multiplicity using the Kohn-Sham formulation [41,42] as implemented in the Vienna Ab-initio Simulation Package (VASP) [43,44]. The interaction of ion cores and electrons was explained using the Projector Augmented Wave (PAW) technique [45, 46]. The generalized gradient approximation (GGA), which is based on the Perdew-Burke-Ernzerhof (PBE) functional [47], was used to handle electron exchange correlation. The rotationally invariant GGA+U approach developed by Dudarev et al. [48] was utilized, with an effective Hubbard parameter U_{eff} being 7.5 eV for the Cu d orbital, as proposed by Arramel et al. [49]. All computations were conducted using plane wave basis sets with a cut-off energy of 500 eV. The Monkhorst-Pack approach was used to establish Brillouin zone sampling to $2\times2\times2$, centered at the Γ point [50]. To accommodate for dispersion correction, the D3 approach with zero-damping [51] was used. The conjugate gradient approach was used to optimize cells. Calculations were judged convergent when the highest stresses on each atom were below 0.01 eV/Å. Throughout the computations, all atoms were permitted to totally relax.

Utilizing DFT+U allows us to obtain the optimized band gap for FASnBr₃ and FASnCl₃. Figure 2 shows the result of DFT band structure and density of states, where the enhanced band gap was 1.667 eV and 2.054 eV, respectively, for FASnBr₃ and FASnCl₃.

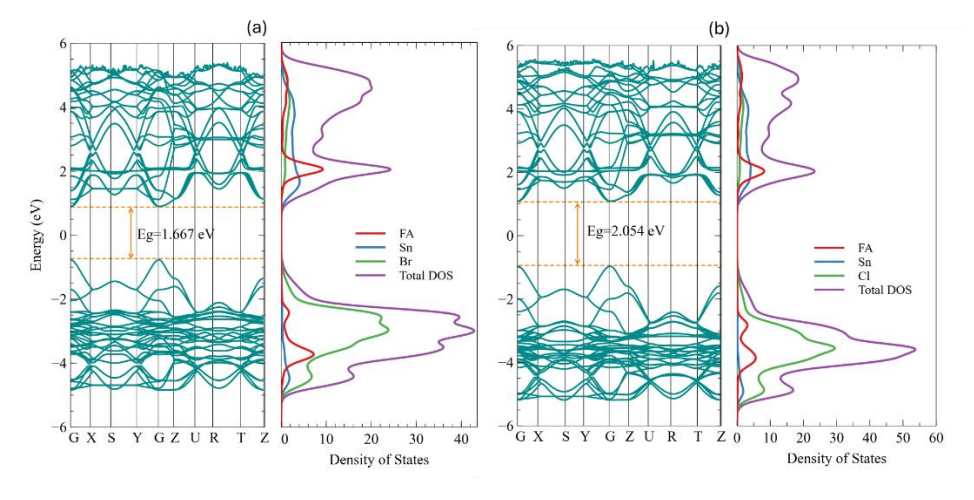


Figure 2 Band Structure and Density of States of (a) FASnBr₃ and (b)FASnCl₃.

3 Results and Discussion

3.1 Implication of Perovskite Layer Thickness on PSC Performance

In this study, we adjusted the perovskite layer thickness between 100 and 600 nm, maintaining all other parameters fixed. Figures 3 and 4 exhibit the J–V properties, external quantum efficiency (EQE) graphs, and the electric characteristics for different thicknesses of FASnX₃ (X = Br, Cl). Figures 3a and 4a illustrate that the thickness of FASnX₃ (X = Br, Cl) active layer affects the J-V characteristics substantially. With the exception of FF, increasing the thickness from 100 to 600 nm yields greater J_{SC} , V_{OC} , and PCE values. This indicates that a larger active layer improves photon absorption and carrier production.

This rise in performance is reflected in the EQE graph shown in Figures 3b and 4b, demonstrating an enhanced ability to absorb visible light in the 300-900 nm range, ultimately boosting the performance of PSCs. An optimum EQE of over 80% is achieved in the visible light wavelength range of 380 to 650 nm for FASnBr₃ and 380 to 500 nm for FASnCl₃. However, beyond a certain thickness, further increasing the FASnX₃ (X = Br, Cl) active layer has no influence on the EQE owing to the constraints of carrier diffusion length.

Figures 3 and 4 show a distinct pattern in the J-V properties, EQE graph, and J-V variables as the thickness of the $FASnX_3$ active layer (X = Br, Cl) raises. The increase is fast from 100 to 600 nm, then slows between 450 and 600 nm. In a thin perovskite layer, the charge carriers' diffusion length exceeds the layer thickness, allowing most extra charge carriers to quickly reach their respective contacts and generate more power [36]. Additionally, studies have shown that a perovskite layer thickness of 400-500 nm ensures effective light absorption with minimal recombination losses [37, 38]. A thickness of 500 nm is recommended for best solar cell performance since bigger perovskite layers have a shorter diffusion length and a higher defect density [35]. Our research revealed that a thickness of 500 nm is suitable for the device, as it reduces the detrimental impacts associated with an exceedingly thick active layer on the collection of photogenerated carriers. At an optimal thickness of 500 nm, the device of both FASnBr₃ and FASnCl₃ demonstrates significantly improved performance. FASnBr₃ has a J_{SC}, V_{OC}, FF, and PCE of 19.60 mA cm⁻², 1.037 V, 74.15 %, and 15.08 %, whereas FASnCl₃ has a J_{SC}, V_{OC}, FF, and PCE of 10.58 mA cm⁻², 1.021V, 75.32 %, and 8.13 %, representing a substantial enhancement compared to the basic parameter results.

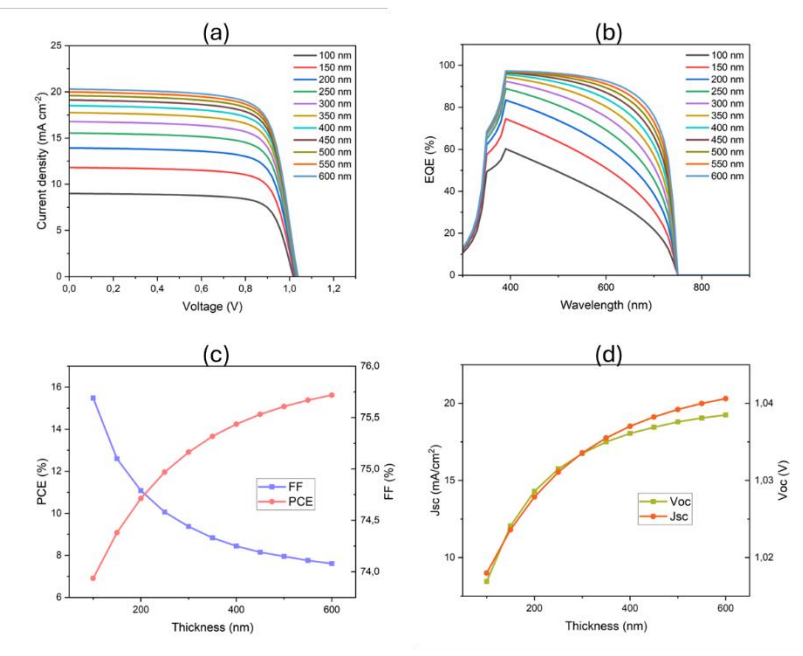


Figure 3 $FASnBr_3$ thickness effect on PSC performance criteria: (a) J-V properties, (b) external quantum efficiency (EQE), (c) FF, PCE, (d) Voc, Jsc.

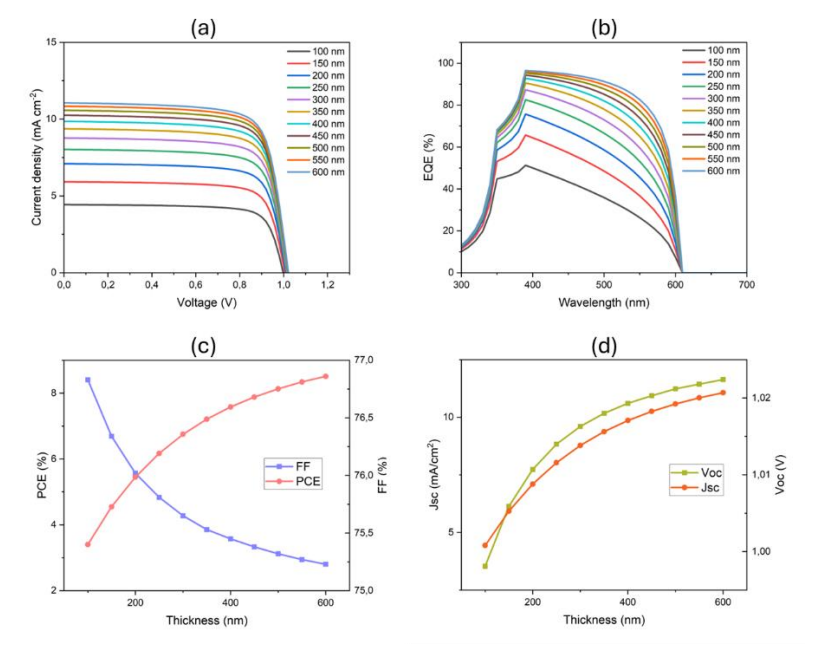


Figure 4 FASnCl₃ thickness effect on PSC performance criteria: (a) J-V properties, (b) external quantum efficiency (EQE), (c) FF, PCE, (d) Voc, Jsc.

3.2 Implication of Defect Density on PSC Performance

To examine the impact of defect density (Nt), we adjusted the absorber layer's Nt between 10^{12} to 10^{20} cm⁻³. The J–V properties, changes in electrical characteristics, and recombination rates for various defect densities are shown in Figures 5 and 6. An increase in defect density impairs PSC performance. Figures 5a and 6a show that when Nt is below 10^{17} cm⁻³, the PSC's J-V properties remain consistent. However, as the defect density surpasses this threshold, the J–V curve degrades dramatically.

The Shockley-Read-Hall (SRH) equation states that increased defect density led to shorter carrier lifetimes, which increases SRH recombination and has a negative impact on V_{OC} and J_{SC} , consistent with the patterns illustrated in Figures 5b and 6b. In contrast, overly large defect densities impede photon absorption, resulting in fewer excitons and lower J_{SC} . As shown in Figures 5c, the PCE drops from 20.53 % to 0.02 % when FASnBr₃ defect density elevates from 10^{12} to 10^{20} cm⁻³, indicating carrier diffusion length $(L = \sqrt{\tau \times D})$.

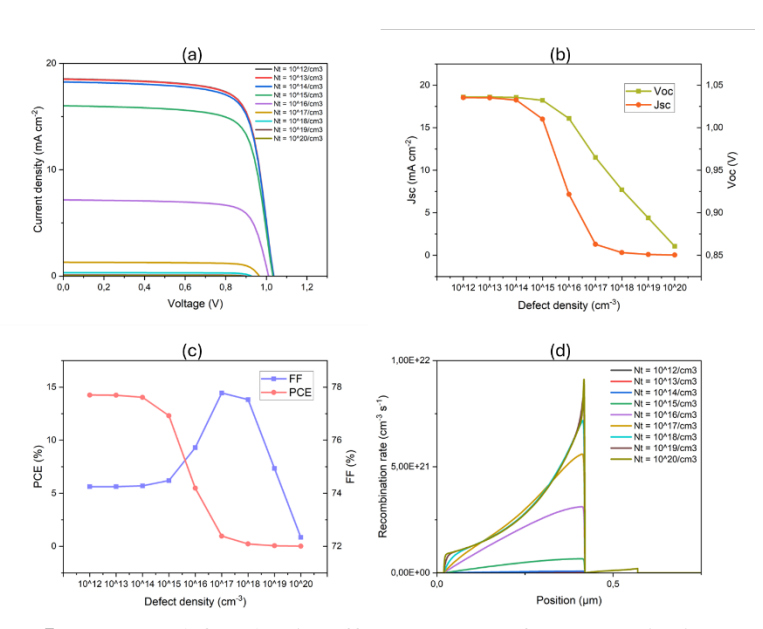


Figure 5 FASnBr₃ defect density effect on PSC performance criteria: (a) J-V properties, (b) Voc, Jsc, (c) FF, PCE, (d) recombination rate.

Figures 5d and 6d indicate that larger carrier defect densities result in shorter carrier diffusion lengths, which increases recombination and reduces carrier lifetimes. This enhanced recombination rate shortens diffusion length, allowing less carriers to reach the interface. It is clear that when *Nt* growss, the device's

overall performance diminishes significantly. Based on our investigation, the desirable defect density (*Nt*) for the absorber layer (FASnBr₃ and FASnCl₃) is 10^{13} cm⁻³.

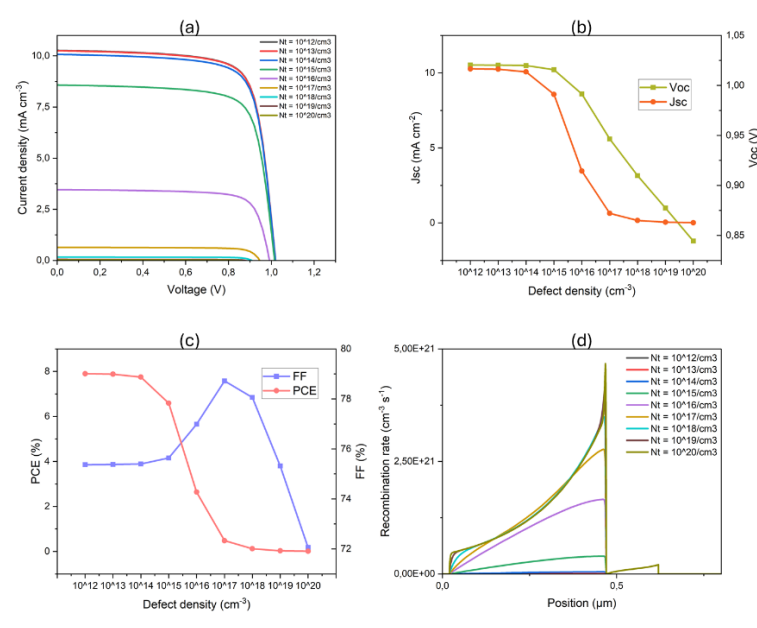


Figure 6 FASnCl₃ defect density effect on PSC performance criteria: (a) J-V properties, (b) Voc, Jsc, (c) FF, PCE, (d) recombination rate.

3.3 Implication of Interface Defect on PSC Performance

To investigate the influence of defects at the PTAA/FASnX₃ (X = Br, Cl) and FASnX₃ (X = Br, Cl)/TiO₂ interfaces on PSC performance, we changed the defect size from 10^{11} to 10^{18} cm⁻². Figures 7 and 8 show the J-V properties for various defect densities at the PTAA/FASnX₃ (X = Br, Cl) and FASnX₃ (X = Br, Cl)/TiO₂ interfaces. Figure 7 shows that as the PTAA/FASnBr₃ interface defect density increased from 10^{11} to 10^{18} cm⁻², the J_{SC} decreased dramatically from 19.99 mA cm⁻² to 0.005 mA cm⁻². However, the V_{OC} only gradually decreased. When the defect density is lower than 10^{16} cm⁻², the performance parameters (J_{SC}, V_{OC}) at the FASnCl₃/TiO₂ interface remain steady. Figure 8 shows that interface defects larger than 10^{16} cm⁻² have a substantial impact. Higher defect concentrations led to reduced cell performance because of increased recombination rates. Accordingly, to obtain optimal performance, we chose an interface defect density of 10^{11} cm⁻² on HTL/AL and 10^{12} cm⁻² on AL/ETL interfaces for both FASnBr₃ and FASnCl₃.

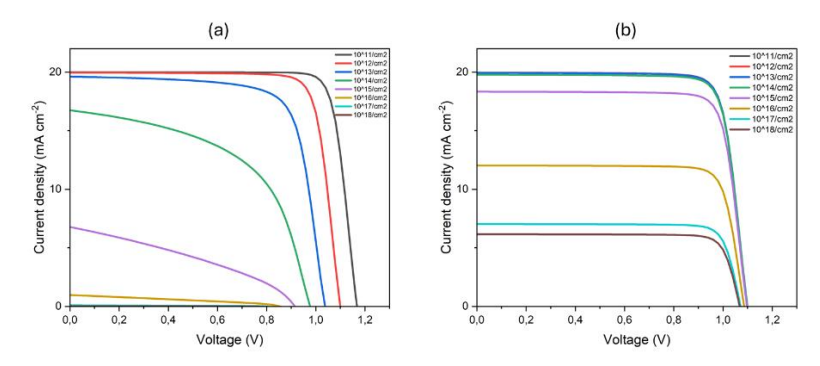


Figure 7 The influence of (a) HTL/FASnBr₃ and (b) FASnBr₃/ETL interface defect on PSC performance J-V characteristics.

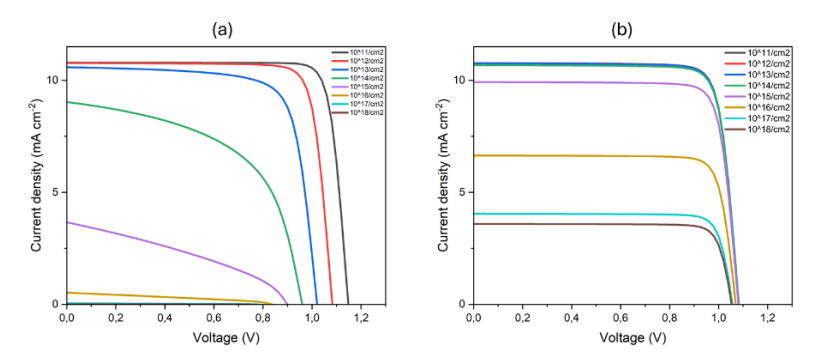


Figure 8 The influence of (a) HTL/FASnCl₃ and (b) FASnCl₃/ETL interface defect on PSC performance J-V characteristics.

Tabel 3 The optimized physical parameters used for the simulation

Material Properties	PTAA	FASnBr ₃	FASnCl ₃	TiO ₂	FTO
Thickness (nm)	20	500	500	150	400
Energy Bandgap (eV)	3.2	1.667 (DFT)	2.054 (DFT)	3.2	3.6
Electron affinity (eV)	2.13	4.2	4.2	4.1	4.1
Dielectric Permittivity	3	8.2	8.2	55	10
CB effective DOS (cm ⁻³)	2 x 10 ¹⁸	2.2 x 10 ¹⁸	2.2 x 10 ¹⁸	1×10^{21}	2.2 x 10 ¹⁸
VB effective DOS (cm ⁻³)	2 x 10 ¹⁸	1.8 x 10 ¹⁹	1.8 x 10 ¹⁹	2×10^{20}	1.8 x 10 ¹⁹
Electron mobility (cm ² /Vs)	10 ⁻³	1.6	1.6	0.006	100
Hole mobility (cm ² /Vs)	10 ⁻³	1.6	1.6	0.006	25
Donor density (cm ⁻³)	0	1.0 x 10 ¹⁹	1.0 x 10 ¹⁹	1.0×10^{21}	1.0×10^{17}
Acceptor density (cm-3)	1.0×10^{17}	0	0	0	0
Defect type	SD	Neutral	Neutral	SA	Neutral
Nt (cm ⁻³)	1.0×10^{15}	1.0×10^{13}	1.0×10^{13}	1.0×10^{15}	1.0×10^{15}

3.4 Overall Performance of PSC

We optimized key variables and discovered that the energy band gap calculated through DFT for FASnBr₃ is 1.667 and 2.054 for FASnCl₃, the active layer of FASnX₃ (X = Br, Cl) should be 500 nm, with a defect density of 10^{13} cm⁻³, an interface defect at ETL/AL of 10^{12} cm⁻², and an interface defect at HTL/AL of 10^{11} cm⁻². Table 3 shows the final settings of the ideal device. The final structure's J-V curve is illustrated in Figure 9, and the inset displays the structure with the highest performance for FASnBr₃ and FASnCl₃, as stated in Table 4.

Voc (V) Jsc (mA/cm2) FF (%) Structures PCE (%) FTO/TiO₂/FASnI₃/PTAA/Au (base) 0.597 27.59 3.92 23.75 FTO/TiO₂/FASnBr₃/PTAA/Au (optimized) 1.167 19,99 84.3 19.67 FTO/TiO₂/FASnCl₃/PTAA/Au (optimized) 1.148 10.79 85.48 10.59

Tabel 4 Final performance of the simulated PSCs

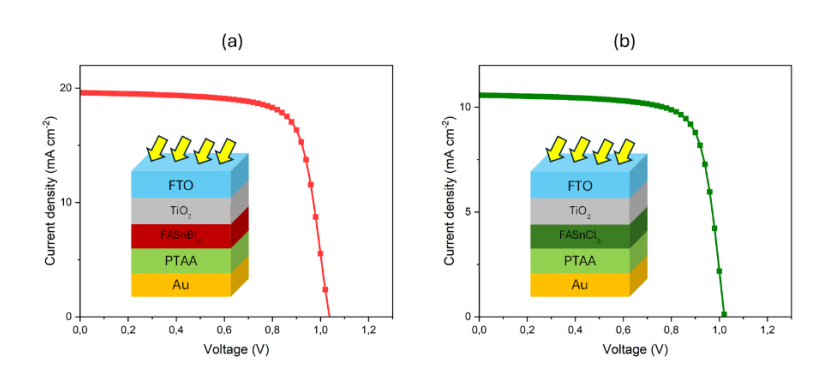


Figure 9 The influence of (a) HTL/FASnCl₃ and (b) FASnCl₃/ETL interface defect on PSC performance J-V characteristics.

4 Conclusion

We have presented a computational study of FASnBr $_3$ and FASnCl $_3$ perovskite solar cells (PSCs) with a configuration of FTO/TiO $_2$ /FASnX $_3$ /PTAA/Au (X = Br, Cl) using SCAPS-1D simulations. We investigated how such characteristics as perovskite active layer thickness, defect density, and interface defect affect solar cell performance. Optimizing these parameters resulted in significant improvements in key PV metrics, including a V $_{OC}$ of 1.167 V, J $_{SC}$ of 19.99 mA cm $^{-2}$, FF of 84.3%, and PCE of 19.67% for FASnBr $_3$ and a V $_{OC}$ of 1.148 V, J $_{SC}$ of 10.79 mA cm $^{-2}$, FF of 85.48%, and PCE of 10.59% for FASnCl $_3$, compared to the initial performance of FASnI $_3$. Furthermore, the results of this investigation

show that FASnBr₃-based PSC outperforms FASnCl₃. To summarize, this simulation work establishes a crucial baseline for constructing cutting-edge FASnX₃-based PSCs and provides researchers with important information for future experimental manipulations and developments.

5 References

- [1] Snaith, H.: Present status and future prospects of perovskite photovoltaics. Nat. Mater. 17, 372 (2018).
- [2] Green, M.A., Ho-Baillie, A., and Snaith, H.J.: The emergence of perovskite solar cells. Nat. Photon. 8, 506 (2014).
- [3] Manser, J.S., Christians, J.A., and Kamat, P.V.: Intriguing optoelectronic properties of metal halide perovskites. Chem. Rev. 116, 2956 (2016).
- [4] Park, N.G., Perovskite solar cells: an emerging photovoltaic technology, Mater. Today 18 (2015) 65–72
- [5] Roknuzzaman, M., Alarco, J.A., Wang, H., Du, A., Tesfamichael, T., Ostrikov, K.(Ken), *Computational Materials Science* (2019) 169
- [6] Kojima, A., Teshima, K., Shirai, Y. and Miyasaka, T. (2009) Organometal Halide Perovskites as Visible-Light Sensitizers for Photovoltaic Cells. Journal of the American Chemical Society, 131, 6050-6051.
- [7] Kim M., Jeong J., Lu H., Lee T.K., Eickemeyer F.T., Liu Y., Choi I.W., Choi S.J., Jo Y., Kim H.-B., *et al.*, Conformal quantum dot-SnO2 layers as electron transporters for efficient perovskite solar cells, Science **375**, 302 (2022).
- [8] Gao W., Chen C., Ran C., Zheng H., Dong H., Xia Y., Chen Y., Huang W. A-site cation engineering of metal halide perovskites: version 3.0 of efficient tin-based lead-free perovskite solar cells Adv. Funct. Mater., 30 (34) (2020)
- [9] Yan Y., Pullerits T., Zheng K., Liang Z., Advancing tin halide perovskites: strategies toward the ASnX₃ paradigm for efficient and durable optoelectronics, ACS. Energy. Lett., 5 (6) (2020), pp. 2052-2086
- [10] Yang, X.-Y. *Photoenergy and Thin Film Materials*; Google Books; John Wiley & Sons: New York, NY, USA, 2019.
- [11] Rühle S., Tabulated values of the Shockley–Queisser limit for single junction solar cells, Solar Energy 130 (2016) 139–147.
- [12] Thomas, A.S. Film Properties Using Metal Salts Washing for Perovskite Solar Cells. Preprints 2022, 2022070192 (doi: 10.20944/preprints 202207.0192.v1).
- [13] Zhao S., Cai W., Wang H., Zang Z., Chen J., Small Methods 2021, 5, 2001308
- [14] Zhou, Y., & Saliba, M. (2021). Zooming in on Metal Halide Perovskites: New Energy Frontiers Emerge. ACS Energy Letters, *6*(8), 2750-2754

- 13
- [15] Hao F., Stoumpos C.C., Cao D.H., Chang R.P.H. and Kanatzidis M.G., Lead-free solid-state organic–inorganic halide perovskite solar cells, Nat. Photonics, 2015, 8, 489.
- [16] Noel N.K., Stranks S.D., Abate A., Wehrenfennig C., Guarnera S., Haghighirad A.A., Sadhanala A., Eperon G. E., Pathak S. K., Johnston M. B., Petrozza A., Herz L. M. and Snaith H. J., Lead-free organic—inorganic tin halide perovskites for photovoltaic applications, Energy Environ. Sci., 2014, 7, 3061.
- [17] Wu L. J., Zhao Y.Q., Chen C.W., Wang L.Z., Liu B. and Cai M. Q., First-principles hybrid functional study of the electronic structure and charge carrier mobility in perovskite CH₃NH₃SnI₃, Chin. Phys. B, 2016, 25, 107202.
- [18] Chung I., Lee B., He J., Chang R.P.H. and Kanatzidis M.G., All-solid-state dye-sensitized solar cells with high efficiency, Nature, 2012, 485, 486.
- [19] Xiao Z., Lei H., Zhang X., Zhou Y., Hosono H. and Kamiya T., Ligand-Hole in [SnI₆] Unit and Origin of Band Gap in Photovoltaic Perovskite Variant Cs₂SnI₆, Bull. Chem. Soc. Jpn., 2015, 88, 1250.
- [20] Koh T.M., Krishnamoorthy T., Yantara N., Shi C.L., We L., Boix P.P., Grimsdale A.C., Mhaisalkar S.G. and Mathews N., Formamidinium tin-based perovskite with low Eg for photovoltaic applications, J. Mater. Chem. A, 2015, 3, 14996.
- [21] Liao M., Yu Bin-Bin, Jin Z., Chen W., Zhu Y., Zhang X., Yao W., Duan T., Djerdj I., and He Z., Efficient and Stable FASnI₃ Perovskite Solar Cells with Effective Interface Modulation by Low-Dimensional Perovskite Layer. ChemSusChem. 2019. 12(22).
- [22] Wu T., Liu X., Luo X., Segawa H., Tong G., Zhang Y., Ono L.K., Qi Y., Han L., Heterogeneous FASnI3 Absorber with Enhanced Electric Field for High-Performance Lead-Free Perovskite Solar Cells, Nano-Micro Lett. (2022) 14:99.
- [23] Ravishankar S., Liu Z., Rau U., Kirchartz T., Multilayer Capacitances: How Selective Contacts Affect Capacitance Measurements of Perovskite Solar Cells, PRX ENERGY 1, 013003 (2022).
- [24] Almufarij R.S., Ashfaq A., Tahir S., Alqurashi R.S., Ragab A.H., El-Refaey D.E., Mushtaq S., Ali Shokralla E., Ali A., Capangpangan R.Y., Alguno A.C., Improving performance and recombination losses in lead free formamidinium tin based perovskite solar cells, Materials Chemistry and Physics 307 (2023) 128150.
- [25] Hosen A., Mian Md. S., and Al Ahmed S.R., Improving the Performance of Lead-Free FASnI₃-Based Perovskite Solar Cell with Nb₂O₅ as an Electron Transport Layer, Adv. Theory Simul. 2023, 6, 2200652.
- [26] Kumar M., Raj A., Kumar A., Anshul A., An optimized lead-free formamidinium Sn-based perovskite solar cell design for high power

- conversion efficiency by SCAPS simulation, Optical Materials 108 (2020) 110213.
- [27] Kahmann S., Nazarenko O., Shao S., Hordiichuk O., Kepenekian M., Even J., Kovalenko M.V., Blake G.R., and Loi M.A., Negative Thermal Quenching in FASnI₃ Perovskite Single Crystals and Thin Films, ACS Energy Lett. 2020, 5, 2512–2519.
- [28] Burgelman M., Decock K., Khelifi S., Abass A., *Thin Solid Films* 2013,535, 296.
- [29] Burgelman M., Nollet P., Degrave S., *Thin Solid Films* 2000, *361–362*, 527.
- [30] Verschraegen J., Burgelman M., Thin Solid Films 2007, 515, 6276.
- [31] Decock K., Khelifi S., Burgelman M., Thin Solid Films 2011, 519, 7481.
- [32] Decock K., Zabierowski P., Burgelman M., J. Appl. Phys. 2012, 111, 043703.
- [33] Ravidas B.K., Roy M.K., Samajdar D.P., Sol. Energy 2023, 249, 163.
- [34] Ke W., Stoumpos C.C., Zhu M., Mao L., Spanopoulos I., Liu J., Chen M., Sarma D., Sci. Adv. 2017;3: e1701293.
- [35] Rai S., Pandey B.K., Dwivedi D.K., Opt Mater. 2020, 100, 109631.
- [36] Singh N.K., Agarwal A., Kanumuri T., Varshney T., in 2020 IEEE Students Conf. on Eng. & Systems (SCES), IEEE, New York City 2020, pp. 1–6.
- [37] Casas G.A., Cappelletti M.A., Cédola A.P., Soucase B.M., E. L. Peltzer Y Blancá, *Superlattices Microstruct*. 2017, *107*, 136.
- [38] Liu F., Zhu J., Wei J., Yi Li, Lv M., Yang S., Zhang B., Yao J., Dai S., *Appl. Phys. Lett.* 2014, *104*, 253508.
- [39] Green, Martin A., et al., Solar cell efficiency tables (Version 61), 2023.
- [40] Kumar M., Raj A., Kumar A., Anshul A., An optimized lead-free formamidinium Sn-based perovskite solar cell design for high power conversion efficiency by SCAPS simulation, Optical Materials 108 (2020) 110213
- [41] Hohenberg, P.; Kohn, W. Inhomogeneous Electron Gas. *Phys. Rev.* 1964, *136*, B864–B871.
- [42] Kohn, W.; Sham, L. J. Self-Consistent Equations Including Exchange and Correlation Effects. *Phys. Rev.* 1965, *140*, A1133–A1138.
- [43] Kresse, G.; Furthmüller, J. Efficiency of Ab-Initio Total Energy Calculations for Metals and Semiconductors Using a Plane-Wave Basis Set. *Comput. Mater. Sci.* 1996, 6, 15–50.
- [44] Kresse, G.; Furthmüller, J. Efficient Iterative Schemes for Ab Initio Total-Energy Calculations Using a Plane-Wave Basis Set. *Phys. Rev. B: Condens. Matter Mater. Phys.* 1996, *54*, 11169–11186.
- [45] Blöchl, P. E. Projector Augmented-Wave Method. *Phys. Rev. B: Condens. Matter Mater. Phys.* 1994, *50*, 17953–17979.

- [46] Kresse, G.; Joubert, D. From Ultrasoft Pseudopotentials to the Projector Augmented-Wave Method. *Phys. Rev. B: Condens. Matter Mater. Phys.*
- [47] Perdew, J. P.; Burke, K.; Ernzerhof, M. Generalized Gradient Approximation Made Simple. *Phys. Rev. Lett.* 1996, 77, 3865–3868.
- [48] Dudarev, S. L.; Botton, G. A.; Savrasov, S. Y.; Humphreys, C. J.; Sutton, A. P. Electron-Energy-Loss Spectra and the Structural Stability of Nickel Oxide: An LSDA+U Study. *Phys. Rev. B: Condens. Matter Mater. Phys.* 1998, *57*, 1505–1509.
- [49] Arramel, Maddalena, F., Mahyuddin, M.H., Yin, X., Tang, C.S., Agusta, M.K., Sahdan, M.F., Diao, C., Dang, C., Birowosuto, M.D., Wee, A.T.S., Rusydi, A., Temperature-induced orbital polarizations and tunable charge dynamics in layered double perovskite thin films, Materials Today Energy 24 (2022) 100921.
- [50] Monkhorst, H. J.; Pack, J. D. Special Points for Brillouin-Zone Integrations. *Phys. Rev. B* 1976, *13*, 5188-5192
- [51] Grimme, S.; Antony, J.; Ehrlich, S.; Krieg, H. A Consistent and Accurate Ab Initio Parametrization of Density Functional Dispersion Correction (DFT-D) for the 94 Elements H-Pu. *J. Chem. Phys.* 2010, *132*, 154104.

Acknowledgment

1999, *59*, 1758–1775.

This work was supported by PT. PLN (Persero) and PT. PLN Nusantara Power. M.H.M. acknowledges a research fund from Institut Teknologi Bandung under the "Riset ITB 2025" scheme. The authors thank Professor Marc Burgelman from the University of Gent for providing and allowing us to utilize the SCAPS-1D simulation program.